Engineering Structures 321 (2024) 118935

Contents lists available at ScienceDirect

Engineering Structures

journal homepage: www.elsevier.com/locate/engstruct

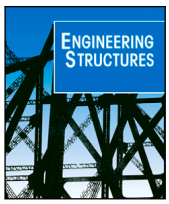

Rotational stiffness of a connection made using a single prestressed bolt

Paweł Pieczka *, Piotr Iwicki

Faculty of Civil and Environmental Engineering, Gdańsk University of Technology, St. Gabriela Narutowicza 11/12, Gdańsk, 80-233, Poland

ARTICLE INFO

Keywords:
Bolted connections
Joint stiffness
Built-up sections
Cold-formed steel
Finite element modeling

ABSTRACT

The often overlooked rotational stiffness of connections utilizing a single prestressed bolt leads to the common assumption of treating such connections as pinned or even modeling them as rigid. Nevertheless, considering the friction between interconnected elements, it is evident that the actual rotational stiffness lies between these simplified assumptions. This study is dedicated to quantifying this stiffness and addressing the question of whether simplifying such connections to pinned or rigid is justifiable. Experimental, theoretical, and numerical analyses were conducted. The results reveal a substantial variability in this phenomenon, which can be effectively described by a normal distribution. Illustrated through a case study involving built-up battened columns, it was demonstrated that the maximum normal force in the column, when considering rotational stiffness of connections, significantly surpasses that obtained for a model assuming pinned connections. This underscores the necessity of employing a model with nonlinear rotational stiffness for an accurate analysis of such constructions.

1. Introduction

Structures composed of cold-formed steel (CFS) elements, despite their wide application and many research conducted in research institutes around the world, are still not fully understood, especially in the context of design. This is due to the wide range of geometric imperfections and the complicated impact of connections on the analysis results. Due to the high sensitivity to local failure, it is necessary to pay special attention to connections in the CFS structures [1].

In engineering practice, designers often simplify structures to beam models with rigid joints. Such joints do not account for the actual axial stiffness. The article [2] presents analyses showing that, to achieve consistency between numerical analyses and experimental results, it is necessary to introduce semi-rigid joints that account for the flexibility of bolted connections of lipped channel braces. In the case of thin-walled structural elements, assuming rigid connections may be unjustified even when using welded joints [3]. Similar attention is required for rotational stiffness.

In the literature, a wide range of approaches to modeling connectors can be found, from those reducing the connector to the point-to-point relationship between the connected parts [4], through those in which the geometry of the connector is simplified using solid elements [5], to those in which the connector is modeled precisely, with an accurately reproduced thread and nut [6,7]. Modern numerical computational models allow for the analysis of joints even up to the point of failure [8]. These analyzes are performed for connections made using both bolts and screws. Zhang et al. [9] presented research on the low closely-spaced built-up members with self-drilling screw connectors.

Bolted connections, where friction plays a significant role, can be divided into two categories: connections subjected to normal force [10–12] and connections subjected to transverse force and bending moment [13,14]. The Eurocode standard [15] describes the procedure for determining the slip resistance of friction joints with preloaded bolts, but this topic still enjoys great popularity among researchers. This is influenced by the complexity of the issue in terms of cyclic durability, as well as the multitude of materials and combinations of bolt arrangements.

Noferesti et al. [16] presented research on ultra-low cycle fatigue evaluation of bolted flange plate moment connections with different amounts of pre-tension in bolts. The research demonstrated a significant impact of bolt pre-tension on the moment resistance and fatigue life. Despite the presence of a total of 14 bolts in the joint, the location of failure in the laboratory connections was at the farthest row of holes from the column. This indicates that in modeling such a connection, it is crucial not only to capture the behavior of the entire group of connectors but also to accurately replicate the influence of individual connectors.

Öztürk and Pul [17] carried out an experimental and numerical study on a full scale apex connection of cold-formed steel portal frames. The rafters made of CFS elements were connected in the middle of the span with a apex profile. The apex profile was a welded I-section

* Corresponding author.
E-mail address: pawel.pieczka@pg.edu.pl (P. Pieczka).

https://doi.org/10.1016/j.engstruct.2024.118935
Received 14 April 2024; Received in revised form 31 July 2024; Accepted 3 September 2024

with the web extended towards the rafters. The entire connection was made with 32 M14-1.5 (8.8) bolts: 16 were located on the upper flange and 16 on the web. The bolts were hand tightened, the hand-tightening torque has been tested. The tightening torque of 100 N m has been found to correspond to a prestressing force of 34 kN. In the numerical model, prestressing force was introduced by shortening the bolt shank. The shortening displacement change calculated by using classical stress–strain equations. The contact between the joined elements with a friction coefficient of 0.3 was defined. Accurate modeling of the prestressed bolts was one of the reasons for the high convergence of the test results with the numerical calculations.

Lim et al. [18,19] carried out an experimental, theoretical, and numerical study to investigate the stiffness and the load capacity of the bolted moment-connections in a CFS portal framing system. By using a group of bolts, it was possible to assume that a single bolt transmits only a shear force, and that the rotational stiffness results from the cooperation of all connectors and largely depends on their spacing. One of the important aspects when designing such connections is the bimoment generated in the CFS element, see also [20]. In this case, the impact of the rotational stiffness of a single bolt may be negligible, but in the case of connections made with a small number of bolts (one or two), the impact may be significant. The rotational stiffness of a joint has a significant impact on the stress distribution in the joined elements.

Aghoury et al. [21] presented research on CFS built-up battened columns. The connection between the batten and the chord was made using two M6 bolts (8.8). Finite element method (FEM) models with and without bolt holes were compared. It was found that the model with holes better reflects the behavior of the tested built-up members. During numerical calculations the rigid connection was assumed. This is an example where more accurate modeling of the joint's rotational stiffness could have a significant impact on the results of numerical calculations. This is due to the low rotational stiffness of the joint used in the study.

Another example of assuming a rigid connection was presented by Mitsui and Sato in the article [22]. Nine types of CFS built-up battened columns, in which the batten–chord connection was made with one prestressed F10T-M12 bolt, were described. The bolts were hand tightened, the hand-tightening torque was not tested. In the article [23] an attempt was made to determine the amplitude of the global initial bow imperfection so that the results of numerical calculations for each column correspond to the resistance obtained from strength tests. Such a dependence turned out to be impossible to determine, the likely reason was the assumption of rigid connections and differences in the prestressing force of individual bolts and the resulting different rotational stiffness of the joints.

The present paper shows experimental tests of the connection made using a single prestressed bolt and focuses on determining the rotational stiffness of such a joint. Such connections can be successfully used in structures made of CFS elements such as built-up columns. The results of the experimental studies were compared with analytical calculations and numerical analyses. This is an innovative aspect of the work because it is usually assumed that these types of connections are pinned or rigid.

2. Analytical approach and experimental work

2.1. Research samples

Experimental tests were carried out on samples representing a full-scale part of a built-up member (geometry similar to the columns presented in [22]). The geometry of the samples is shown in Fig. 1. The chord was made of a 2 mm thick cold-formed channel section. Each chord sample has six holes for fixing in the test base and ten holes for testing bolted connections. The channel section is made of S350GD+Z200 steel. A 200 g/m^2 zinc coating by the continuous hot-dip galvanizing process provides a 14 μm thick coating by design. This coating is widely used because of its long-term corrosion resistance.

The battens were made of flat bars with dimensions of 6×35×200 mm, using S235 steel. After the bolt holes were made, the battens were hot-dip galvanized. M12 bolts (10.9 - ISO 7412) for prestressed connections were used for the batten–chord connections. The built-up members made of the elements described above, due to the complete separation of the steel cores from environmental factors, are permanently protected against corrosion.

Table 1
Parameters of the roughness profile of the research samples.

	Ra (μm)		Rq (μm)		Rz (μm)	
	Mean	SD	Mean	SD	Mean	SD
Chord	0.68	0.26	0.93	0.41	5.12	2.40
Batten	1.69	1.12	2.15	1.45	10.19	6.00

2.2. Coefficient of friction

Before testing the rotational stiffness of the bolted joint, the coefficient of friction between the batten and the chord was tested. The coefficient of friction depends on the roughness of the contact surfaces and the material they are made of. In the case of both types of samples, the outer surface is a zinc coating, but due to differences in the galvanization method, it is not identical. Using the Mitutoyo Surftest SJ-210 meter, the roughness of selected samples was tested. For each sample, measurements were made on four paths parallel to the direction of force. The basic parameters describing surface roughness are the arithmetical mean height of the roughness profile (R_a), the root mean square deviation of the roughness profile (R_q) and the maximum height of the roughness profile (R_z). The mean values and standard deviations (SD) of the parameters of the roughness profile of the research samples were summarized in Table 1. 57 chord samples and 37 batten samples were tested. Not all chord samples tested for roughness were used in the friction study.

The static coefficient of friction can be calculated as the ratio of the friction force to the normal force between the tested samples. The concept of determining the coefficient of friction proposed by Amontons (1699) was described, among others, by Wójcik and Frączek [24]. The results of 37 friction force tests are shown in Fig. 2. A significant dispersion of results may result from the high variability of the thickness and roughness of the zinc coating. The average value of the coefficient of friction between the batten and the chord was calculated as the slope of the line describing the linear regression from all measurement points: $\mu_{mean} = 0.22$. This value corresponds to class D according to the EN 1090-2 standard, i.e. for untreated surfaces [25]. It is also possible to calculate the minimum and maximum friction coefficients for the tested samples: $\mu_{min} = 0.13$, $\mu_{max} = 0.30$.

In the literature, there are examples of deriving relationships between the surface roughness profile and the friction coefficient for steel specimens (see, e.g., [26,27]). Fig. 3 shows the roughness parameters of a surface depending on a friction coefficient obtained in the experimental tests for all pairs of elements. Based on the charts, a clear relationship between surface roughness parameters and the friction coefficient cannot be determined.

Zheng et al. [26] showed that the relationship determined for steel samples subjected to various surface preparation processes cannot be applied to samples coated with an additional layer (in the presented case: powder coating or anti-slip coating). This is due to the different mechanisms through which forces are transferred between the attached surfaces than in the case of uncoated surfaces, and this issue requires further investigation.

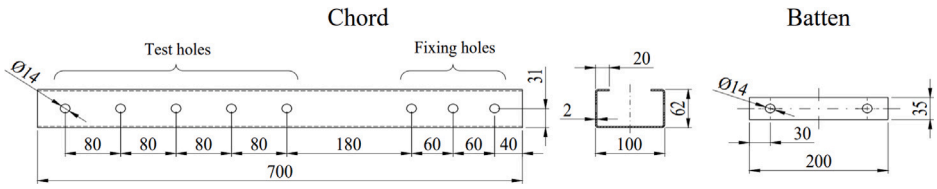

Fig. 1. Research samples.

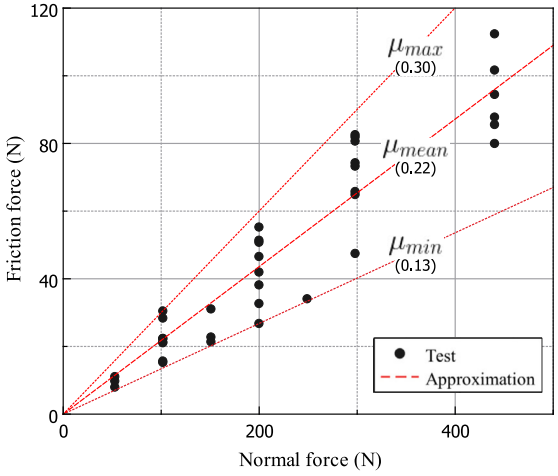

Fig. 2. Coefficient of friction between the research samples.

2.3. Rotational stiffness

The rotational stiffness of a connection made with a single bolt results from friction between the joined sheets caused by the prestressing force. Fig. 4 shows the diagrams of the friction areas of samples subjected to a normal force or a bending moment. In the first case, it is customary to assume that the stiffness of the joint and the resistance to slip are independent of the size of the contact surface, but only of the prestressing force (F_P), the coefficient of friction (μ) and the number of the slip surfaces (n_b) [6].

Assuming a uniform stress distribution from the prestressing force, it is possible to determine the shear stresses τ_{slip} at which rotational slip occurs:

$$\tau_{slip} = \frac{\mu F_p}{A} = \frac{\mu F_p}{\pi(r_2^2 - r_1^2)} \tag{1}$$

where r_1 and r_2 are the inner and outer radii of the pressure area, respectively, and A is the pressure area on the contact surface (see Fig. 4(b)).

The moment resistance for one slip surface under pure bending (without shear force) can be calculated according to Eq. (2):

$$M_{slip,pure} = \tau_{slip}\, W_\phi \tag{2}$$

where W_ϕ represents the slip surface section modulus:

$$W_\phi = \int_{r_1}^{r_2} 2\pi r^2\, dr = \frac{2\pi}{3}(r_2^3 - r_1^3) \tag{3}$$

It is also possible to take into account the shear force V that occurs simultaneously with the moment M. In this case, it can be assumed that the rotation occurs after reaching the limit value of the shear stress induced by both components. The shear stresses can be calculated according to Eq. (4).

$$\tau = \frac{M}{W_\phi} + \frac{V}{A} \tag{4}$$

If the moment is caused by a single concentrated force applied at a distance e_V from the axis of rotation, there is a linear relationship between the moment M and the shear force in the joint: $M = V \cdot e_V$. Eq. (4) can then be written as:

$$\tau = M\left(\frac{1}{W_\phi} + \frac{1}{Ae_V}\right) \tag{5}$$

By transforming Eq. (5), a formula for the slip moment that takes the shear force into account can be derived:

$$M_{slip,V} = \tau_{slip}\left(\frac{1}{W_\phi} + \frac{1}{Ae_V}\right)^{-1} = \mu\, F_p\, \frac{W_\phi\, e_V}{W_\phi + Ae_V} \tag{6}$$

Rotation of the joint requires slippage in two planes: the contact surface between the batten and the chord, and any other plane, e.g. the plane between the nut and the washer or the plane between the bolt head and the washer. Due to the recommended lubrication or oiling of the bolt and nut [25], it can be assumed that slippage in the planes in contact with these elements occurs without friction. However, this does not affect the contact surface between the connected plates. Considering the above, the moment described by Eq. (6) can be considered sufficient for the rotation of the entire joint.

The research was carried out on a stand designed for a simple bending test of the chord–batten connection, as shown in Fig. 5. The test setup was designed in such a way that multiple tests could be conducted on a single branch, in each test a new batten was bolted to the chord at an unused hole. The M12 bolts were tightened using the controlled torque method with a torque wrench (Proxxon PR23353). The nuts were coated with molybdenum disulfide paste. The force was applied using a hydraulic press (Zwick 500) at a distance of 110 mm from the rotation axis. The displacement of the machine piston was force-controlled at a rate of 25 N/s.

Tightening the M12 bolt with a torque of 100 N m permits the assumption of a prestressing force of 50 kN [28]. Substituting into Eqs. (3) and (6): r_1 equal to the radius of the hole (7 mm), r_2 equal to the outer radius of the washer increased by the thickness of the thinner sheet (14 mm), μ equal to the mean coefficient of friction specified in Section 2.2 and the prestressing force described above, the moment required for slipping is equal to 109 N m. For the minimum and maximum friction coefficients, the moment can be obtained as 65 and 148 N m, respectively.

A total of 61 tests were performed (after this number it was concluded that conducting further tests did not provide additional conclusions). In each test, the dependence of the bending moment on the angle of rotation (M–Φ) was measured indirectly. The moment was calculated on the basis of the force obtained from the testing machine, and the angle of rotation was calculated on the basis of the displacement of the end of the batten measured with an inductive displacement sensor.

The M–Φ relationship from a sample study is shown in Fig. 6(a). For further analysis, the M–Φ curves from the individual tests were simplified by a piecewise linear approximation created by reading the moment values for rotations of 0.005, 0.025, and 0.060 radians. All samples exhibited a decrease in stiffness with progressive rotation of the joint. In the final phase of the test, the moment increase became negligibly small. Therefore, beyond a rotation value of 0.060 radians, no further increase was assumed. The exhaustion of the bending capacity resulted from exceeding the limit shear stresses in the friction zone,

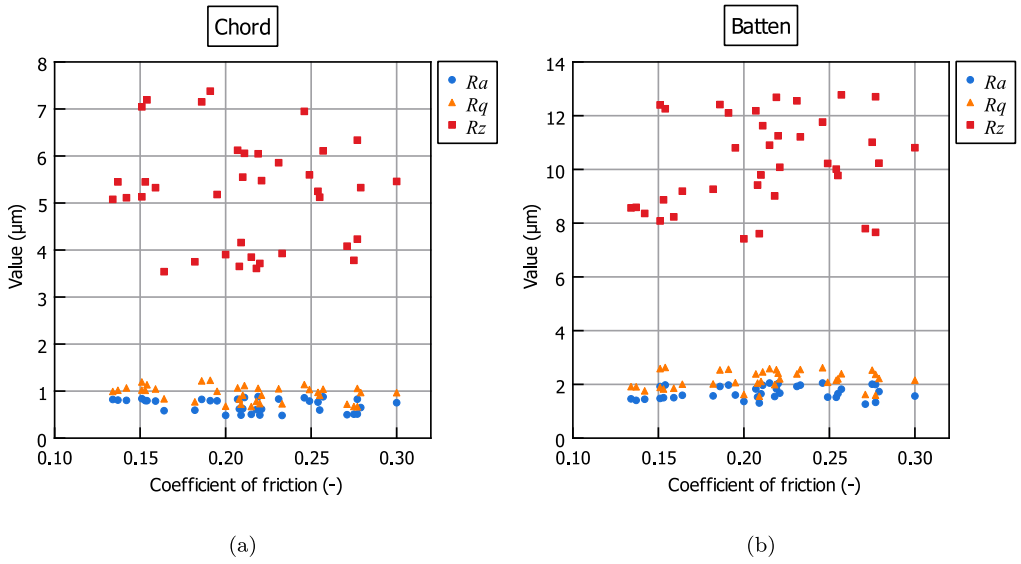

Fig. 3. Surface roughness parameters depending on the friction coefficient obtained in the experimental tests: (a) chord; (b) batten.

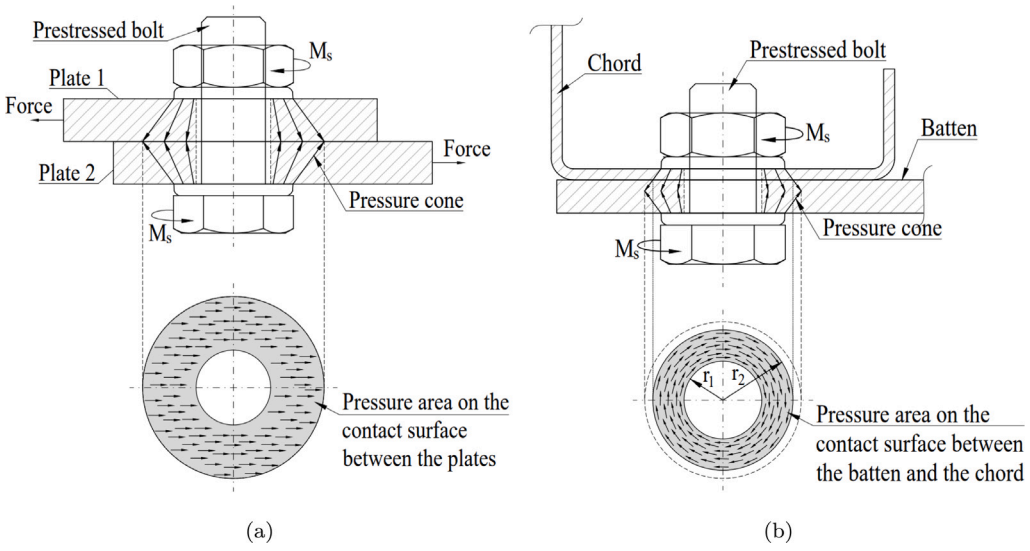

Fig. 4. Friction area for elements subjected to: (a) normal force; (b) bending moment.

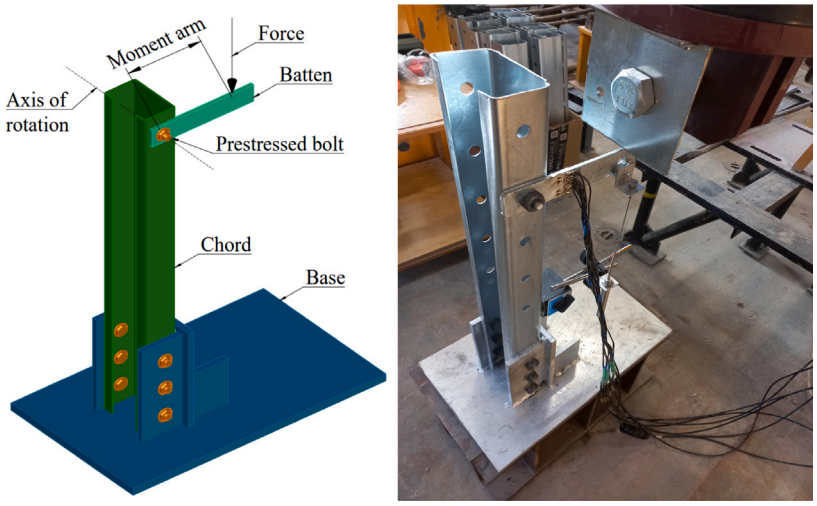

Fig. 5. Test setup.

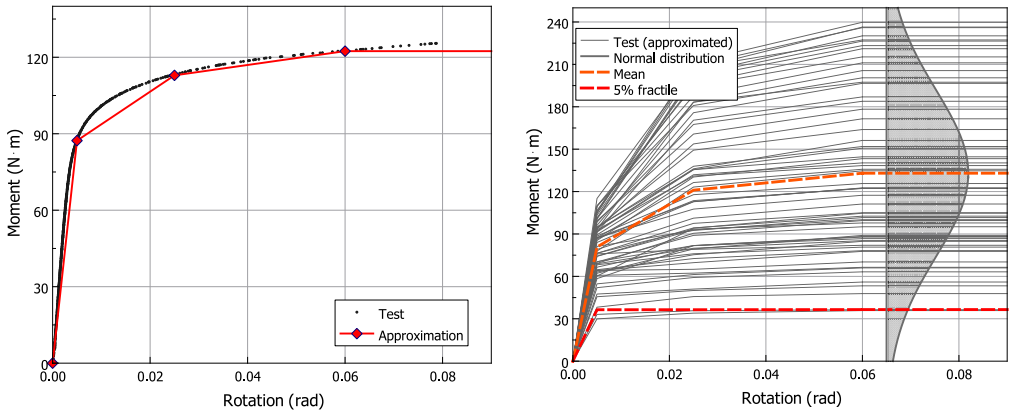

Fig. 6. Rotational stiffness results: (a) piecewise linear approximation of an example measurement; (b) presentation of approximated results from all tests.

Table 2
Rotational stiffness — experimental results.

Rotation (rad)	Moment (N m)		
	Mean	SD	5% fractile
0.005	80.8	20.3	36.4
0.025	121.0	51.6	36.4
0.060	133.0	58.8	36.5

and further rotation resulted from slippage. No other causes, such as buckling, were observed.

Fig. 6(b) presents the approximations from all tests as well as the curve calculated as the average of all tests. Significant discrepancies were observed between the results of the individual tests. During the investigation of the causes of these discrepancies, the correlation between the roughness profile of the batten and chord (described in Section 2.2) and the rotational stiffness in each test was examined. However, no such relationship was found. An additional factor that could influence the rotational stiffness was the thickness of the zinc coating. Fig. 6(b) also shows a curve describing the normal distribution for the limit moment of each sample. Based on the normal distribution, it is possible to calculate the moment value corresponding to the 5% fractile. Table 2 presents the mean values, standard deviations, and 5% fractile values of the moment for the characteristic points of the piecewise linear approximation.

For selected samples, tests were conducted with the use of strain gauge sensors. The strain gauges were placed on both sides of the batten in a cross-section 40 mm away from the axis of rotation. The analysis of the sensor data showed a stress distribution consistent with an analytical, linearly varying distribution due to the bending of the batten. Due to the lack of stress variability along the axis defined by the thickness of the batten, it is reasonable to conclude that, for the assessment of the bending moment, mounting sensors on only one side is sufficient.

3. Numerical analyses

The test specimen was simulated by means of software ABAQUS [29]. The FE model of the sample was established based on nominal dimensions. The model consisted of a section of the chord with a length of 200 mm, the batten, and the bolt along with the nut and two washers. The bolt was modeled as non-threaded with a core thickness shank. All parts were modeled using the C3D8R element (an 8-node linear brick, reduced integration, hourglass control). The element size in the contact zone was 0.3–1.0 mm. To reduce computation time, elements outside the contact zone were larger in size, but did not exceed 5 mm. At least four elements were used through the thickness of the plates, see Fig. 7.

The material property values were introduced on the basis of standard recommendations for the respective steel grades [1,15,30]. The Young's modulus E and the Poisson's ratio ν were taken as 210 GPa and 0.3, respectively, for all elements. The yield strength f_y, the ultimate strength f_u, and the limit plastic elongation ε_u were defined. For the S235 steel batten, they were as follows: $f_y = 235$ MPa, $f_u = 360$ MPa, $\varepsilon_u = 0.15$. For the S350GD+Z200 steel chord, they were: $f_y = 350$ MPa, $f_u = 420$ MPa, $\varepsilon_u = 0.15$. For the 10.9 class bolt, the strength parameters were: $f_y = 900$ MPa, $f_u = 1000$ MPa, and the limit plastic elongation $\varepsilon_u = 0.02$ was set based on articles [31,32] in which it was shown that this is a safe value for constructions at room temperature.

In the contact zone between the batten and the chord, surface-to-surface contact was implemented (see Fig. 7) with the main friction coefficient μ_1 in the tangential direction. In the remaining parts of the model, a general contact with the secondary friction coefficient μ_2 was defined, taking into account all contacting elements. Due to the use of the bolt coated with molybdenum disulfide paste in the tests, the friction coefficient of $\mu_2 = 0.05$ was assumed. For the entire model, "hard" contact was declared in the normal direction. Three models with friction coefficients μ_1 determined in Section 2.2 were made. Additionally, the value of μ_1 was determined for which the limit moment from the FEM analysis corresponds to the 5% fractile value obtained from the experimental tests ($\mu_1 = 0.05$).

The analysis was divided into 2 steps. In the first step, the bolt was preloaded using the "bolt load" function. This function models the tightening of the bolt so that it carries a specified load. A prestressing force of 50 kN was introduced. The chord was fixed in a cross-section located 150 mm from the axis of rotation of the joint. Additional point supports were introduced in each element to prevent instabilities during the analysis of the unloaded parts.

In the second step, a vertical force was applied to the upper surface of the batten. This force was distributed over a 6×6 mm area, with the center of the loaded zone located on the arm 110 mm relative to the rotation axis. To maintain the preload on the bolt obtained in the first step, the length of the bolt was fixed. In the second step, only the boundary conditions placed on the chord were retained.

The model was solved using nonlinear large-displacement elasto-plastic analysis (static, general). In step 2, the applied force was increased until the solution convergence was lost. The calculation was interrupted when the limit load was reached.

Fig. 8 shows the results of the FEM analysis for the model ($\mu_1 = 0.22$; $\mu_2 = 0.05$). The rotation in the joint occurs through slippage in two contact planes: between the batten and the chord, and between the batten and the washer. The chord did not undergo significant deformation

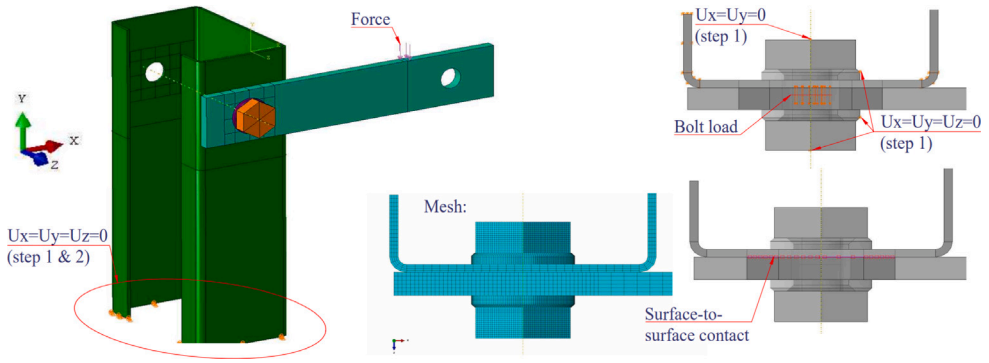

Fig. 7. FE model of the tested joint.

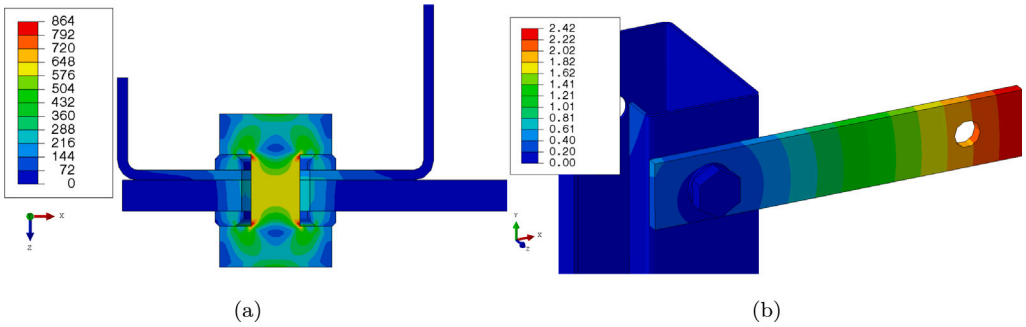

Fig. 8. FEM analysis results for the model ($\mu_1 = 0.22$; $\mu_2 = 0.05$): (a) Von Mises stress (MPa) after preloading in the cross-section at the axis of rotation of the joint; (b) displacement (mm) at the moment of computation interruption for step 2.

or buckling during the rotation of the joint. The force–displacement relationship was converted into the moment–rotation angle of the joint. The maximum moment was 123.7 N m at the joint rotation angle of 0.014 radians.

The stress contours on both sides of the batten in a cylindrical coordinate system are presented in Fig. 9. The stresses in the area around the hole reach the yield point. The moment in the joint is the integral of the shear stresses on both lateral surfaces of the batten. Due to the assumed friction coefficients, the values of shear stresses (S23 in the cylindrical coordinate system) on the side of the chord (inner) are significantly greater than those obtained on the side of the washer (outer). The distribution of shear stresses is rotationally symmetric, and the size of the area subjected to stresses due to bolt prestressing corresponds to that assumed in the analytical model.

The influence of the eccentricity between the axis of the bolt and the center of the holes in the connected elements was also examined. This was implemented by creating models with the bolt displaced by 1 mm in 4 directions (X+, X-, Y+, Y-, see Fig. 7). In each case, both the limit moment and the initial stiffness were similar to the results obtained for the model without eccentricity.

4. Summary of research and analysis results

Fig. 10 presents a summary of the rotational stiffness for the examined joint from analytical calculations, FEM analyzes, and the piecewise linear approximations from measurements. Assuming the average friction coefficient obtained from the experiments ($\mu_{mean} = 0.22$), the maximum bending moments in the joint obtained from both the FEM and analytical models are similar to the mean value from the experimental tests.

The rotational stiffness close to the 5% fractile value obtained from the experimental tests is achieved in the FE model by applying a friction coefficient of $\mu_1 = \mu_2 = 0.04$. This value corresponds to surfaces subjected to lubrication or oiling.

The results presented in Fig. 10 pertain to the investigated chord–batten joint and, beyond the rotational stiffness itself, also take into account the flexibility of the both elements and the load eccentricity. The batten is subjected to bending about its stronger axis, while the chord is subjected to bidirectional bending along with compression. The impact of the flexibility of these elements can be estimated by conducting additional numerical analyses with a significantly increased Young's modulus value assigned to the material of these elements. Fig. 11 shows a comparison of the initial rotational stiffness for models with a Young's modulus of $E = 210$ GPa and with a modulus increased 1000 times, a value sufficiently high that the deformation of the chord and batten becomes negligibly small (marked on the graph as $E = \infty$). The analyzes were performed for the two models described in Section 3: FEM ($\mu_1 = 0.22$; $\mu_2 = 0.05$), FEM ($\mu_1 = 0.13$; $\mu_2 = 0.05$).

The analyses showed that the flexibility of the chord and batten constitutes a significant portion of the entire system's flexibility in the initial phase of rotation. The corrected initial rotational stiffness is 5.4 and 3.8 times greater than the uncorrected stiffness. However, after exceeding 0.010 radians of rotation, this influence ceases to be significant due to the exhaustion of the slip resistance in the contact zone. Taking into account the above conclusions in the analysis of the experimental results, it is possible to introduce corrected rotational stiffness by increasing the initial rotational stiffness (e.g. shifting the horizontal coordinate of the first characteristic point on the M–Φ graph from 0.005 rad to 0.002 rad increases the initial stiffness by 2.5 times).

Additionally, it is also possible to transition from rotational stiffness that includes the influence of shear force to the stiffness of pure rotation. For this purpose, the relationships contained in Eqs. (2) and (6) can be used. For the discussed joint, the difference amounts to 10%. However, this would require introducing separate stiffness related to the shear force into the model and the interaction between these stiffnesses.

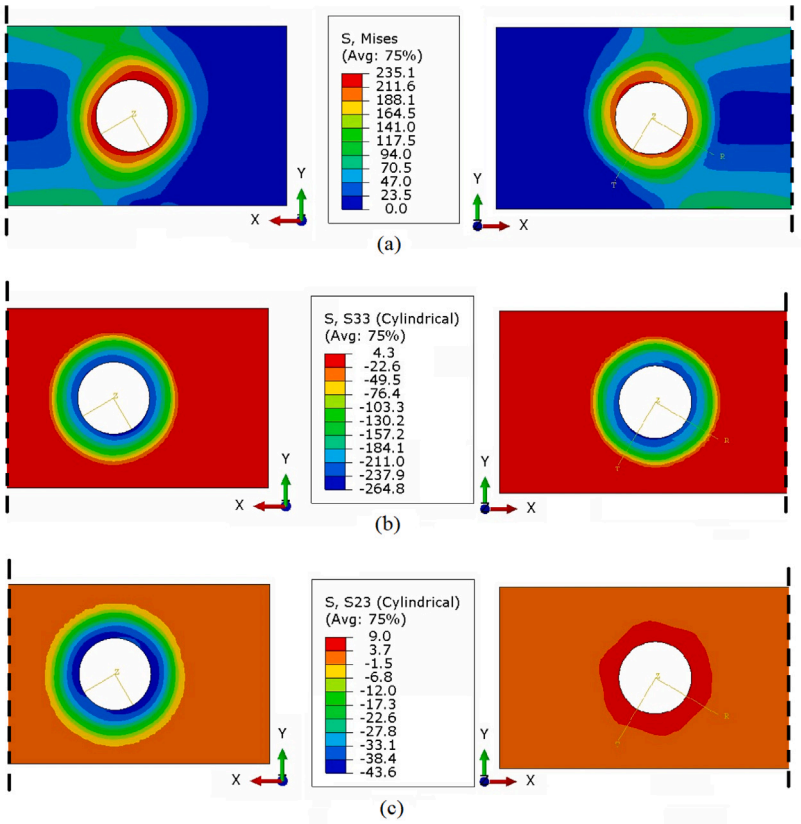

Fig. 9. Stress (MPa) contours for the batten (model: $\mu_1 = 0.22$; $\mu_2 = 0.05$) (on the left for the inner side, on the right for the outer side): (a) Von Mises stress; (b) normal stress S33 - parallel to the bolt axis; (c) shear stress S23 in a cylindrical coordinate system.

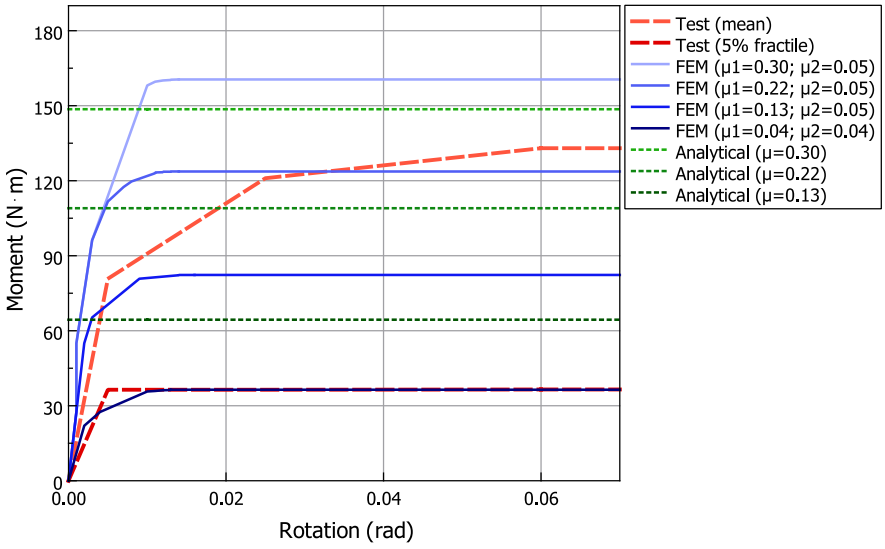

Fig. 10. Summary of the rotational stiffness results.

5. Application example

The obtained rotational stiffnesses can be applied, for example, in models of built-up columns in which the connection between the chord and the batten is made using a single prestressed bolt. Columns with such joints were studied by Mitsui and Sato [22]. Finite element analyzes were performed for example columns: $L3700a400h60$ and $L3700a720h60$ (the length of the member $L = 3700$ mm, the axial separation between the battens $a = 400$ mm or $a = 720$ mm, and the distance between the centroids of the chords $h = 60$ mm, other dimensions are assumed as in the article [22], and presented in Fig. 12).

A numerical shell model of the column with rigid connections (entire contact surface connected using the "tie" function [29]) between battens and chords was described in the article [23]. For comparison purposes, similar models were created, but the connection was made using the "fastener" function [29]. Four types of connections were modeled: Rigid, Pinned, and two Semi-Rigid with nonlinear rotational stiffness determined in the experiments: mean and 5% fractile (corrected as recommended in Section 4). The remaining components of

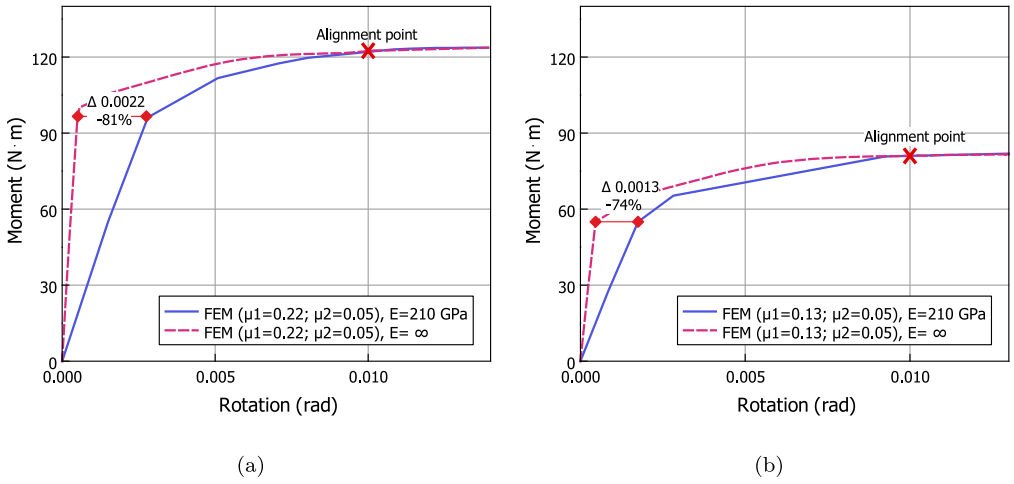

Fig. 11. The impact of the flexibility of the chord and the batten on the initial rotational stiffness.

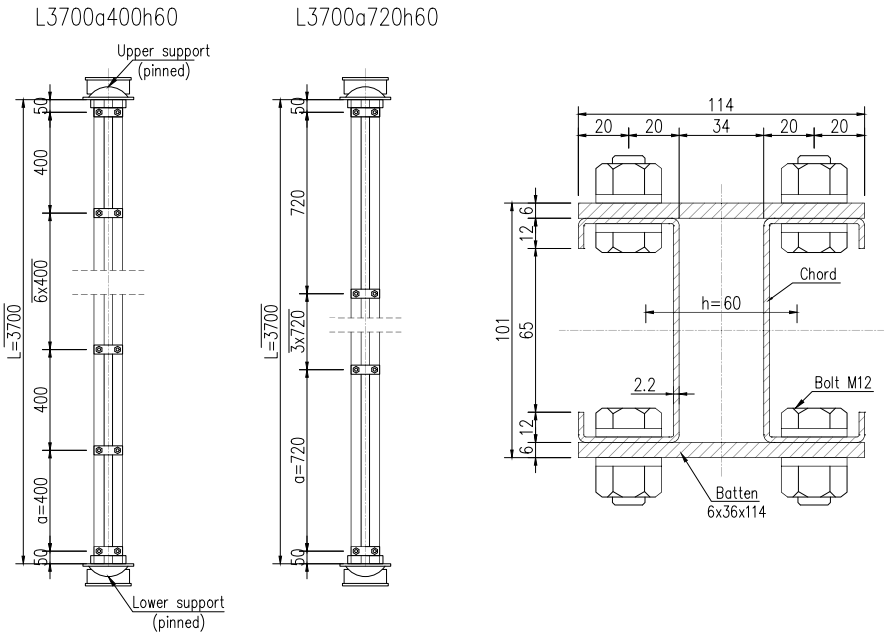

Fig. 12. Cross-section and views of columns $L3700a400h60$ and $L3700a720h60$.

the relative motion of the connector were set as rigid. The physical radius of influence was set to 14 mm (analogously to r_2 in Section 2.3), implying that nodes on both the chord and the batten within this radius from the joint axis are associated with the fastener. The motion of the attachment point is then coupled in a weighted sense to the motion of the nodes in this region by a distributed coupling constraint.

Geometrically and materially nonlinear static analyses were carried out, taking into account an initial global bow imperfection with an amplitude equal to $L/500$ (7.4 mm). The analysis was carried out as a static general with displacement control, and the normal force in the column was induced by displacing the upper support towards the lower support. The results of the analysis are presented in Fig. 13. The graph also presents the results of the experimental studies described in the article [22]. In this context, displacement refers to the change in distance between the upper and lower supports.

The initial stiffness was uniform for all FEM models. The maximum forces established in the studies for models with semi-rigid connections were higher than those obtained for models with pinned connections. Introducing the stiffness corresponding to the 5% fractile from the experimental tests increased the column's load-bearing capacity by 5.4% and 12.2%. In the case of stiffness corresponding to the mean value from the studies, the increases were 17.7% and 29.4%. Greater increases were obtained for the $L3700a400h60$ column due to the smaller spacing of the battens, and therefore a greater number of connections. Based on this, it can be concluded that this stiffness is not negligibly small, and proper modeling may lead to greater agreement between research results and numerical analysis results. The difference between the results of models with rigid and semi-rigid connections is also significant. Simplifying the model by introducing rigid connections leads to a significantly increased load-bearing capacity of the entire columns.

Comparing the results of FEM analyses and experiments reveals discrepancies in initial stiffnesses, which may result from the flexibility of the experimental setup. The maximum normal force values from the tests do not correspond to those obtained from FEM models. This discrepancy arises from the fact that, in addition to joint stiffness, a significant factor affecting the load-bearing capacity of built-up columns in FEM calculations is the introduced imperfections. In the article [23], analyses of the influence of the amplitude of the bow imperfection introduced in FEM models on the load-bearing capacity results due to

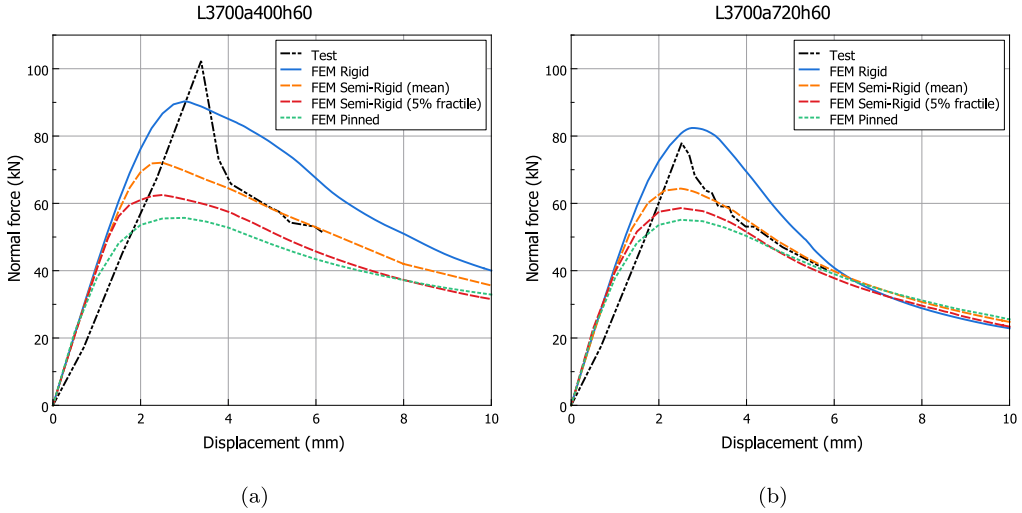

Fig. 13. The force–displacement relationship for two example built-up columns, from FEM calculations depending on the assumed rotational stiffness of the connections, and from the experimental tests [22].

axial compression were conducted for 9 types of columns described in [22]. Assuming rigid joints, the imperfection amplitudes required to obtain convergence between the test results and the measurements ranged from $L/800$ to $L/250$.

6. Conclusions

The rotational stiffness and the maximum bending moment of the joint made using one M12 prestressed bolt were tested. Analytical and numerical models of the joint were developed.

On the basis of the research, it was determined that the statistical variability of the discussed stiffness is significant, even though the samples came from the same batch of materials and the connections were made in the same way. It was not possible to determine the relationship between the surface roughness parameters of the joined elements and the friction coefficient. Therefore, this phenomenon was treated as random and described by a normal distribution.

Using the example of a numerical analysis of built-up battened columns, it was shown that the maximum normal force in the column for models with nonlinear, semi-rigid rotational stiffness of connections (determined on the basis of the experimental tests) is significantly higher than that obtained for a model with pinned connections (up to 30%). The impact of this stiffness increases with the number of joints in the structure. The initial assumptions that the stiffness of such a joint is insufficient to model it as rigid were also confirmed. These conclusions highlight the necessity of using a model with semi-rigid connection stiffness for a proper analysis of such structures.

Further analyses are necessary to determine the value of rotational stiffness suitable for application in numerical models. Possible approaches include:

- using a conservative stiffness, previously defined as: Test (5% fractile),
- applying the mean stiffness (not recommended for structures with a small number of joints),
- incorporating a random distribution of stiffness in the model based on a normal distribution.

In addition, further research on the discussed topic is possible, for example, concerning joints with larger bolts or the use of additional friction elements to increase rotational stiffness.

CRediT authorship contribution statement

Paweł Pieczka: Writing – original draft, Visualization, Software, Resources, Project administration, Methodology, Investigation, Funding acquisition, Conceptualization. **Piotr Iwicki:** Writing – review & editing, Supervision, Methodology, Conceptualization.

Declaration of competing interest

The authors declare that they have no known competing financial interests or personal relationships that could have appeared to influence the work reported in this paper.

Data availability

The data that support the findings of this study are available on request from the corresponding author.

Acknowledgments

Financial support of these studies from Faculty of Civil and Environmental Engineering Gdańsk University of Technology by the Grants for Young Scientists. The numerical calculations were performed using the computing resources of CI TASK at Gdańsk University of Technology.

References

[1] CEN/EN. EN 1993-1-3: Eurocode 3: Design of steel structures - Part 1-3: General rules - Supplementary rules for cold-formed members and sheeting. 2006.
[2] Gusella F, Orlando M, Peterman K. Stiffness and resistance of brace-to-upright joints with lipped channel braces assembled flange-to-flange. J Constr Steel Res 2022;193:107258. http://dx.doi.org/10.1016/j.jcsr.2022.107258.
[3] Roure F, Peköz T, Somalo MR, Bonada J, Pastor MM, Segura A. Cross-aisle stiffness analysis of industrial welded cold-formed steel rack upright frames. Thin-Walled Struct 2019;141:332–44. http://dx.doi.org/10.1016/j.tws.2019.04.041.
[4] Abbasi M, Khezri M, Rasmussen K, Schafer B. Elastic buckling analysis of cold-formed steel built-up sections with discrete fasteners using the compound strip method. Thin-Walled Struct 2018;124:58–71. http://dx.doi.org/10.1016/j.tws.2017.11.046.
[5] Lyu Y-F, Wang Y-B, Li G-Q, Jiang J. Numerical analysis on the ultimate bearing resistance of single-bolt connection with high strength steels. J Constr Steel Res 2019;153:118–29. http://dx.doi.org/10.1016/j.jcsr.2018.10.006.
[6] Ye J, Quan G, Kyvelou P, Teh L, Gardner L. A practical numerical model for thin-walled steel connections and built-up members. Structures 2022;38:753–64. http://dx.doi.org/10.1016/j.istruc.2022.02.028.

[7] Hu Y, Shen L, Nie S, Yang B, Sha W. FE simulation and experimental tests of high-strength structural bolts under tension. J Constr Steel Res 2016;126:174–86. http://dx.doi.org/10.1016/j.jcsr.2016.07.021.
[8] Quan G, Ye J, Li W. Computational modelling of cold-formed steel lap joints with screw fasteners. Structures 2021;33:230–45. http://dx.doi.org/10.1016/j.istruc.2021.04.062.
[9] Zhang L, Zhou T, Li Y, Sang L. Research on the post-buckling strength of screw composite thin plate with large deflection. Structures 2021;32:204–15. http://dx.doi.org/10.1016/j.istruc.2021.02.065.
[10] Zhou Z, Zhou X, Zhou Q, Guo W, Huang W. Development and experimental validation of a novel friction-type energy dissipation steel truss. J Constr Steel Res 2023;211:108150. http://dx.doi.org/10.1016/j.jcsr.2023.108150.
[11] Zhou Q, Liu S, Zhou Z, Guo W, Huang W, He W, et al. Experimental and numerical studies on friction energy-dissipating combination chord of staggered truss. J Constr Steel Res 2024;213:108403. http://dx.doi.org/10.1016/j.jcsr.2023.108403.
[12] Gao J, Wang C-L, Meng S, Zeng B. Performance evaluation of friction dampers considering different metal pairs and loading rates. J Constr Steel Res 2023;204:107859. http://dx.doi.org/10.1016/j.jcsr.2023.107859.
[13] Seifan F, Mirghaderi SR, Ghassemieh M. A new friction-slip connection for moment frames with continuous beams. J Constr Steel Res 2020;175:106337. http://dx.doi.org/10.1016/j.jcsr.2020.106337.
[14] Shahini MF, Bagheri Sabbagh A, Davidson P, Mirghaderi R, Torabian S. Experiments on cold-formed steel moment-resisting connections with bolting friction-slip mechanism. J Constr Steel Res 2022;196:107368. http://dx.doi.org/10.1016/j.jcsr.2022.107368.
[15] CEN/EN. EN 1993-1-8: Eurocode 3: Design of steel structures - Part 1-8: Design of joints. 2005.
[16] Noferesti H, Razmkhah MH, Gerami M. Laboratory and ultra-low cycle fatigue evaluation of the seismic performance of BFP connection with different amounts of pre-tension in bolts. J Constr Steel Res 2024;212:108295. http://dx.doi.org/10.1016/j.jcsr.2023.108295.
[17] Öztürk F, Pul S. Experimental and numerical study on a full scale apex connection of cold-formed steel portal frames. Thin-Walled Struct 2015;94:79–88. http://dx.doi.org/10.1016/j.tws.2015.04.004.
[18] Lim J, Nethercot D. Stiffness prediction for bolted moment-connections between cold-formed steel members. J Constr Steel Res 2004;60(1):85–107. http://dx.doi.org/10.1016/S0143-974X(03)00105-6.
[19] Lim JB, Hancock GJ, Charles Clifton G, Pham CH, Das R. DSM for ultimate strength of bolted moment-connections between cold-formed steel channel members. J Constr Steel Res 2016;117:196–203. http://dx.doi.org/10.1016/j.jcsr.2015.10.005.
[20] Rinchen, Rasmussen KJ. Numerical modelling of cold-formed steel single C-section portal frames. J Constr Steel Res 2019;158:143–55. http://dx.doi.org/10.1016/j.jcsr.2019.03.024.
[21] El Aghoury M, Salem A, Hanna M, Amoush E. Ultimate capacity of battened columns composed of four equal slender angles. Thin-Walled Struct 2013;63:175–85. http://dx.doi.org/10.1016/j.tws.2012.07.019.
[22] Mitsui K, Sato A. Flexural elastic buckling stress of batten type light gauge built-up member. Civ Environ Eng Rep 2017;25(2):161–72. http://dx.doi.org/10.1515/ceer-2017-0027.
[23] Pieczka P, Iwicki P. Numerical analysis on axial capacity of steel built-up battened columns. Arch Civ Eng 2022;68(No 2):655–77. http://dx.doi.org/10.24425/ace.2022.140665.
[24] Wójcik A, Frączek J. The problem of standardising the static friction force measurement in plant granular materials. Powder Technol 2022;398:117133. http://dx.doi.org/10.1016/j.powtec.2022.117133.
[25] CEN/EN. EN 1090-2: Execution of steel structures and aluminium structures - Part 2: Technical requirements for steel structures. 2018.
[26] Zheng B, Wang J, Gu Y, Shu G, Xie J, Jiang Q. Experimental study on stainless steel high-strength bolted slip-resistant connections. Eng Struct 2021;231:111778. http://dx.doi.org/10.1016/j.engstruct.2020.111778.
[27] Wang Y-B, Wang Y-Z, Chen K, Li G-Q. Slip factor between shot blasted mild steel and high strength steel surfaces. J Constr Steel Res 2020;168:105969. http://dx.doi.org/10.1016/j.jcsr.2020.105969.
[28] DIN. DIN-18800: Steel structures – Part 7: Execution and constructor's qualification. 2008.
[29] Abaqus/CAE. User's manual. 2020.
[30] CEN/EN. EN 1993-1-1: Eurocode 3: Design of steel structures — Part 1-1: General rules and rules for buildings. 2005.
[31] Li J, Xin H, Correia JA, Berto F, Zhao B, Bo Y, et al. Mesh size effects on fracture locus of high strength bolts: A mesoscale critical equivalent plastic strain (MCEPS) approach. Eng Fail Anal 2022;138:106385. http://dx.doi.org/10.1016/j.engfailanal.2022.106385.
[32] Ban H, Yang Q, Shi Y, Luo Z. Constitutive model of high-performance bolts at elevated temperatures. Eng Struct 2021;233:111889. http://dx.doi.org/10.1016/j.engstruct.2021.111889.